Linear optical properties of strained $(Si)_n/(Ge)_n$ superlattices on (001) Si substrates

E. Ghahramani
Department of Physics and Ontario Laser and Lightwave Research Centre, University of Toronto, Toronto, Ontario, Canada M5S 1A7

D. J. Moss
National Research Council of Canada, Ottawa, Canada K1A 0R6

J. E. Sipe
Department of Physics and Ontario Laser and Lightwave Research Centre, University of Toronto, Toronto, Ontario, Canada M5S 1A7

(Received 30 May 1989; revised manuscript received 14 September 1989)

We report the first full band-structure calculation of the linear optical properties of strained $(Si)_n/(Ge)_n$ superlattices on Si(001) substrates for $n=2,3,4$. We use a semi-*ab initio* minimal basis orthogonalized linear combination of Gaussian orbitals technique, in conjunction with a linear analytic tetrahedra method, to obtain $\vec{\epsilon}(\omega)$. We find that the expected anisotropy in these novel materials is large and almost entirely due to the strain in Ge rather than to the lower symmetry of the superlattices compared to the bulk materials; in a simple picture it results from an alignment of more bonds (antibonds) along the superlattice axis than perpendicular to it. The pure superlattice features are only observed near the absorption edges, they differ from superlattice to superlattice, and are the real signature of each superlattice. Most of the features of the response function at frequencies away from the absorption edge are found to be due to bulklike transitions.

I. INTRODUCTION

The fundamental understanding of the electronic and optical properties of superlattices has presented new and interesting challenges in both theoretical and experimental physics. From a more practical point of view, the possibility of designing structures which exhibit desired optical or electronic properties is very intriguing. In recent years the strained $(Si)_n/(Ge)_n$ (001) series of superlattices, in particular, have received a great deal of attention.[1-8] This is partly because of their interesting physical features such as the effect of the strain on the band gap, and the possibility of growing a direct-band-gap superlattice from constituent materials which have indirect band gaps. Also, the prospect of interfacing these superlattices grown on a silicon substrate with silicon-based technology seems feasible.

Much of the theoretical work[1-5] on these superlattices has been concerned with understanding the electronic band structures. The related experimental work[6-8] consists mainly of electroreflectance measurements. Although such measurements are particularly sensitive to transitions at critical points, they do not yield information on transitions at all frequencies. Our main goal in the present work is threefold: (1) to obtain quantitative values for the dielectric tensor of these materials over a wide range of frequencies, (2) to understand the source of the anisotropy in the dielectric tensor, and (3) to study linear optical properties near the absorption edges, where one expects these properties to differ from bulklike properties due to new transitions to the folded bands.

The calculation of $\vec{\epsilon}(\omega)$ requires the knowledge of energies and momentum matrix elements throughout the entire Brillouin zone. In the past, the linear combination of Gaussian orbitals (LCGO) technique has been used to calculate the band structures of a variety of bulk materials.[9-15] In the direct-space version of the LCGO method, both the orbitals and effective single-site potentials are expanded in terms of Gaussians.[1,9,10,13-15] This expansion allows for the analytic evaluation of the Hamiltonian and overlap matrix elements in real space,[16,17] which facilitates the computation. The method, and slight variations of it, have been used by a number of researchers to calculate a wide range of electronic properties of different materials.[1,9,10,13-17]

Huang *et al.*[14] have used a semi-*ab initio*, minimal-basis, direct-space LCGO method to calculate the band structures of group-IV elemental and III-V compound semiconductors. The results of these calculations, between the range -15 to 10 eV, have been compared with experimental values for bulk Si and Ge.[14] Their results for the valence and lower conduction bands are in good agreement with experiment. In a recent publication[1] we demonstrated that a semi-*ab initio*, minimal-basis LCGO technique, in conjunction with the $X\alpha$ (Refs. 14 and 17) method for constructing the potentials of the constituent bulk materials of the strained $(Si)_n/(Ge)_n$ superlattices ($n=2,3,4,5$) on Si(001), can be used to calculate the band structure of these superlattices. In our implementation of the LCGO method the local single-site effective potentials and basis functions for bulk Si and Ge are constructed by adjusting the α for each bulk material

to produce the correct lowest bulk band gap. We then use these bulk orbitals and potentials to construct the superlattice basis and effective potentials. In this manner we do not do any fitting to the superlattice properties. The band gaps that result from the calculation should thus be identified with the observed transitions, in contrast to self-consistent density-functional calculations where the band gaps must be adjusted with quasiparticle corrections,[2] or more approximately by an upward shift in the conduction bands.[3-5] For all the superlattice band structures in the present work we find the band gap to be indirect. Our calculations[1] are in good agreement with experimental results.[6-8]

In the present work we have used essentially the same approach to construct the Hamiltonian and overlap matrix elements for each superlattice, which are then used within a "supercell" scheme to obtain the band-structure and momentum matrix elements. We employ the linear analytic tetrahedra method (LATM) of Gilat and Raubenheimer and of Lehnmann and Taut[18] to evaluate the frequency-dependent dielectric tensor.

The results of our LATM calculation of the $\vec{\epsilon}(\omega)$ indicate that the optical anisotropy in the superlattices is large. We show that the main features of the $\vec{\epsilon}(\omega)$ at frequencies far from the superlattice absorption edges are almost entirely due to bulklike transitions. In particular, most of the anisotropy is due to strain in the Ge. We also argue that the larger response in the direction of the superlattice axis can be attributed to a greater alignment of the bonds (antibonds) in this direction. The pure superlattice features are only observed near the absorption edges. These features differ from superlattice to superlattice, and are the real signature of each superlattice.

The paper is organized as follows. In Sec. II we give a brief description of the band-structure calculations. In Sec. III, the results of our calculation of the $\vec{\epsilon}(\omega)$ using these bands and employing the LATM are presented. We analyze these results and discuss the source and the size of the large anisotropy, and the absorption edge behavior, in Sec. IV.

II. BAND-STRUCTURE CALCULATIONS

The details of the direct-space LCGO method have been adequately discussed in the literature.[1,9,19,13-17] Below we give a summary of this approach and other details relevant to our problem.

The crystal charge density for each *constituent bulk material* is estimated at a large number of points in real space from the superposition of the Hartree-Fock atomic wave functions.[14,19] The exchange-correlation potential is then constructed using the $X\alpha$ method, by setting the parameter α for each *bulk* material to produce the correct lowest-energy band gap of that material. This is done by initially choosing some reasonable value for α and constructing the exchange-correlation potentials according to the Hohenberg-Kohn-Sham local-density-functional approximation.[14,20] The total effective bulk crystal potential then is written as superposition of effective single-site potentials $V(\mathbf{r})$. Using a least-squares-fitting procedure the effective single-site potential for each bulk material is then expanded as follows:

$$V(\mathbf{r})=-\frac{Z}{|\mathbf{r}|}e^{-\beta r^2}+\sum_w \mathcal{C}_w e^{-\gamma_w r^2}, \tag{2.1}$$

where Z and $\mathcal{C}_w$ are the expansion coefficients and differ for each type of atoms; β and γ_w are Gaussian exponents. Usually nine Gaussians are sufficient to provide a good fit up to a radial distance of about 8 a.u. Typically 12 Gaussians for each bulk material are used. The first term in Eq. (2.1) describes the short-range behavior of the Coulomb potential.

Next, s-type ($e^{-\alpha_i r^2}$), p-type ($xe^{-\alpha_i r^2}$, etc.), and d-type ($xye^{-\alpha_i r^2}$, etc.) Gaussian orbitals are used to construct the contracted atomiclike orbitals as follows:

$$\Phi_{pqs}(\mathbf{r})=\sum_n \mathcal{D}_{pqs,n} G(\alpha_n,\mathbf{r},pq,s,), \tag{2.2}$$

where $G(\alpha_n,\mathbf{r},p,q,s)=x^p y^q z^s e^{-\alpha_n r^2}$ are the Gaussian functions and $\mathcal{D}_{pqs,n}$ are the expansion coefficients to be determined. The index n runs over the number of Gaussians included in the expansion of each orbital type; typically 14 Gaussians per orbital are used for each bulk material. The exponents of these Gaussians are chosen to range between $\alpha_1=0.15$ to $\alpha_{14}=250\,000$. Note that in the minimal orbital scheme the basis for Si consists of nine orbitals ($1s,2s,2p,3s,3p$) and for Ge 18 orbitals ($1s,2s,2p,3p,3d,4s,4p$). The expansion coefficients are determined by solving the Schrödinger equation with the single-site potential $V(\mathbf{r})$. Once the basis orbitals are determined, the Hamiltonian matrix elements for a wave vector $\mathbf{k}$, at which the lowest-energy band gap for each bulk material occurs, are constructed as follows. The contributions from the single-site potentials are summed, and added to the kinetic term to form the total crystal Hamiltonian. The Hamiltonian matrix elements are obtained by expressing the Hamiltonian operator in the nonorthogonal basis of the Bloch states, which, for a given $\mathbf{k}$, are formed from the atomiclike orbitals. The Hamiltonian matrix thus formed is then diagonalized. If the lowest-energy band gap for each bulk material is not in agreement with experimental value, a new α for that material is chosen and the process is repeated until the correct value is obtained. We note that this is not, of course, a self-consistent procedure.

Note that the above functional form of the single-site potential and basis functions allows analytic evaluation of the all the multicenter integrals involved in the calculation.[15,16] The analytical form of these integrals are given in Appendix A.

Once the single-site potential and atomic-like orbitals for each constituent bulk material are known we proceed to calculate the band structure of the strained $(\mathrm{Si})_n/(\mathrm{Ge})_n$ superlattices on Si (001) substrate as follows. We expand the semi-*ab initio* bulk silicon and germanium single-site potentials over the appropriate lattice sites of each superlattice. The superlattice atomic-like basis is taken as the direct sum of the constituent bulk atomic-like basis. These orbitals are then used to form Bloch states. Using these Bloch states the superlattice Hamiltonian and overlap matrix elements within a "supercell" scheme are constructed. In this scheme the overlap matrix elements are given by

$$[S_{\Lambda,\Delta}]_{i_\Lambda j_\Delta} = \sum_{s(\Lambda,\Delta)} e^{i\mathbf{k}\cdot\mathbf{R}_s(\Lambda)} \sum_m \sum_n \mathcal{D}_{i,m}\mathcal{D}_{j,n} \times \int d\mathbf{r}\, G(\alpha_m, \mathbf{A}, p_1, q_1, s_1) G(\alpha_n, \mathbf{B}, p_2, q_2, s_2) , \tag{2.3}$$

and the Hamiltonian matrix elements are given by

$$\begin{aligned}[H_{\Lambda,\Delta}]_{i_\Lambda j_\Delta} = \sum_{\mathbf{R}_s(\Lambda)} e^{i\mathbf{k}\cdot\mathbf{R}_s(\Lambda)} \sum_m \sum_n \mathcal{D}_{i,m}\mathcal{D}_{j,n} \times \Bigg[& \int d\mathbf{r}\, G(\alpha_m, \mathbf{A}, p_1, q_1, s_1)(-\tfrac{1}{2}\nabla^2) G(\alpha_n, \mathbf{B}, p_2, q_2, s_2) \\ & - \sum_{\Omega(\Lambda)} Z(\Omega) \sum_{u(\Lambda,\Omega)} \int d\mathbf{r}\, G(\alpha_m, \mathbf{A}, p_1, q_1, s_1) \\ & \qquad \times \frac{\exp\{-\beta(\Omega)[\mathbf{r}-\mathbf{R}_u(\Lambda,\Omega)]^2\}}{|\mathbf{r}-\mathbf{R}_u(\Lambda,\Omega)|} G(\alpha_n, \mathbf{B}, p_2, q_2, s_2) \\ & + \sum_{\Omega(\Lambda)} \sum_{u(\Lambda,\Omega)} \sum_w \mathcal{C}_w(\Omega) \int d\mathbf{r}\, G(\alpha_m, \mathbf{A}, p_1, q_1, s_1) \\ & \qquad \times \exp\{-\gamma_w(\Omega)[\mathbf{r}-\mathbf{R}_u(\Lambda,\Omega)]^2\} \\ & \qquad \times G(\alpha_n, \mathbf{B}, p_2, q_2, s_2) \Bigg] , \end{aligned} \tag{2.4}$$

where Λ and Δ each refer to different atomic types. Vectors $\mathbf{R}_s(\Lambda)$, which are centered on an atom Λ in the central unit supercell, locate the centers of all the other supercells labeled by s. The collective indices $i_\Lambda \equiv \{p_1, q_1, s_1\}_\Lambda$ and $j_\Delta \equiv \{p_2, q_2, s_2\}_\Delta$ label the different types of orbitals on atoms Λ and Δ, respectively, while indices m and n indicate the different Gaussian orbitals used in the expansion of the wave functions. Index Ω labels the different atomic planes perpendicular to the superlattice axis $\hat{z}$ and vectors $\mathbf{R}_u(\Lambda,\Omega)$ locate the atomic sites, labeled by u, on the Ωth plane and are centered on the Λ atom in the central supercell. The potential expansion coefficients for the atoms on the Ωth atomic plane, $Z(\Omega)$ and $\mathcal{C}_w(\Omega)$, and the corresponding exponent $\beta(\Omega)$ and $\gamma_w(\Omega)$, are defined in Eq. (2.2)

Typically we restrict vectors $\mathbf{R}_u(\Lambda,\Omega)$ to lie within a sphere of radius equivalent to eight nearest neighbors from the central atom Λ. The lattice sums over $\mathbf{R}_s(\Lambda)$ must be carried to full convergence. We include interactions up to seven nearest neighbors, from the central atom, Λ, in the summation. Adding in further neighbors changes the calculated energy values by less than 0.001 eV.

To simplify the calculation, we reduce the dimensions of the Hamiltonian and overlap matrix elements by orthogonalizing the valence Bloch states of each atom in the supercell to the core Bloch states of *all* the atoms in the unit cell. Within the minimal number of orbitals scheme we identify the core and valence states of Si as $(1s, 2s, 2p)$ and $(3s, 3p)$, respectively, while for Ge the core and valence states are $(1s, 2s, 2p, 3s, 3p, 3d)$ and $(4s, 4p)$, respectively. For example, for $(Si)_4/(GE)_4$ the Hamiltonian and overlap matrices are 108×108 ($[9+18]\times4=108$) before orthogonalization to the core states and 32×32 ($[4+4]\times4=32$) after. The Hamiltonian is then diagonalized in the orthogonalized basis. The diagonalization of these smaller matrices typically lead to energies within 0.02 eV of what would be obtained from a full calculation.[10] The full details of orthogonalization are given in Appendix B.

Once the eigenvalues and eigenstates of the superlattice Hamiltonian are obtained, the momentum matrix elements can be constructed. These matrix elements are given by

$$\begin{aligned}\mathbf{P}_{L,M} &= \langle \Psi_L | \hat{\mathbf{P}} | \Psi_M \rangle \\ &= \sum_{i,j} W^*_{Li} W_{Mj} \sum_{s(\Lambda,\Delta)} e^{i\mathbf{k}\cdot\mathbf{R}_s(\Lambda)} \sum_m \sum_n \mathcal{D}_{i,m}\mathcal{D}_{j,n} \int d\mathbf{r}\, G(\alpha_m, \mathbf{A}, p_1, q_1, s_1)(-i\hbar\nabla) G(\alpha_n, \mathbf{B}, p_2, q_2, s_2) , \end{aligned} \tag{2.5}$$

where L and M label the eigenstates of the Hamiltonian and W is the unitary matrix which transforms the Bloch states to the eigenstates of the Hamiltonian.

The band structures of strained $(Si)_n/(Ge)_n$ superlattices on Si(001) for $n=2,3,4$ along certain directions in the Brillouin zone (see Fig. 1) are given in Fig. 2 and the direct and indirect band gaps are summarized in Table I.

TABLE I. Band gaps (from this calculation) for $(Si)_n/(Ge)_n$ superlattices in eV.

Superlattice	Direct gap	Indirect gap
$(Si)_2/(Ge)_2$	1.87	0.78
$(Si)_3/(Ge)_3$	1.22	0.77
$(Si)_4/(Ge)_4$	1.37	0.78

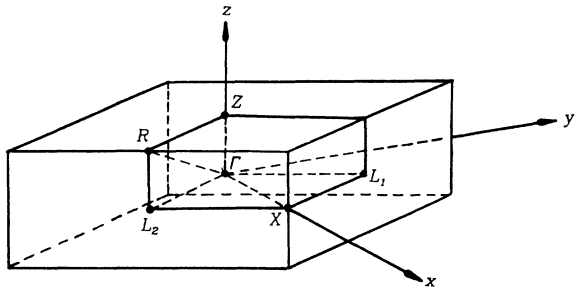

FIG. 1. The strained $(Si)_4/(Ge)_4$ superlattice Brillouin zone and its irreducible segment.

We have already discussed the important features of these bands and compared our results[1] with experimental values[6,7] and the results of other theoretical calculations.[2] The overall agreement is good (see Table III of Ref. 1). However, we have pointed out[1] that use of a minimal basis leads to small inaccuracies in the band structure. A case in point is the small magnitude of the splitting of the first and second pairs of the zone-folded states of Si_4Ge_4, at Γ, in the present calculation (see Fig. 2). With minimal basis LCGO we observe these splitting magnitudes to be about 0.01 and 0.03 eV, respectively, com-

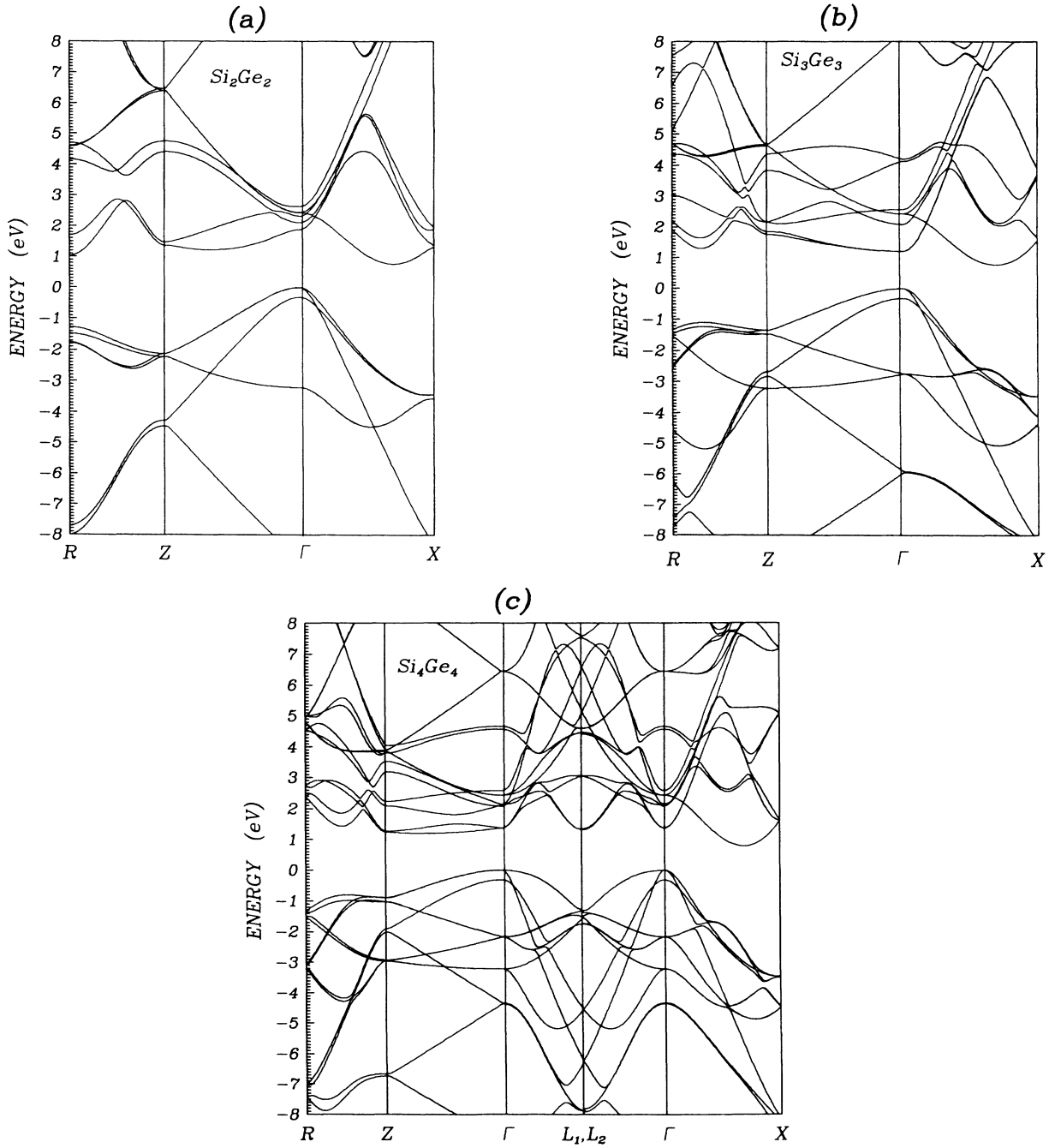

FIG. 2. Energy band structure of the strained $(Si)_n/(Ge)_n$ superlattices. (a) $(Si)_2/(Ge_2$, (b) $(Si)_3/(Ge_3)$, (c) $(Si)/_4/(Ge)_4$ (note that the interface bonds lift the fourfold symmetry about the crystal axis, rendering points L_1 and L_2 distinguishable).

TABLE II. Critical points at Γ for $(Si)_4/(Ge)_4$ (the labels have been described in the text). $|\langle v|P^T|c\rangle|^2 \equiv \frac{1}{2}(|\langle v|P_x|c\rangle|^2+|\langle v|P_y|c\rangle|^2)$.

Transition	ΔE (eV)	$\lvert\langle v\rvert P^T\rvert c\rangle\rvert^2$ (a.u.)	$\lvert\langle v\rvert P_z\rvert c\rangle\rvert^2$ (a.u.)	Critical point
$\Gamma_{1v}^T \rightarrow \Gamma_{1c}^{ZF}$	1.37	0.0	0.0	M_1
$\Gamma_{2v}^T \rightarrow \Gamma_{1c}^{ZF}$	1.38	0.0	0.0	M_1
$\Gamma_{v}^z \rightarrow \Gamma_{1c}^{ZF}$	1.69	0.0	0.0	M_1
$\Gamma_{1v}^T \rightarrow \Gamma_{2c}^{ZF}$	1.38	0.001	0.0	M_0
$\Gamma_{2v}^T \rightarrow \Gamma_{2c}^{ZF}$	1.39	0.001	0.0	M_0
$\Gamma_{v}^z \rightarrow \Gamma_{2c}^{ZF}$	1.70	0.0	0.002	M_0
$\Gamma_{1v}^T \rightarrow \Gamma_{3c}^{ZF}$	2.05	0.0	0.0	M_1
$\Gamma_{2v}^T \rightarrow \Gamma_{3c}^{ZF}$	2.06	0.002	0.0	M_2
$\Gamma_{v}^z \rightarrow \Gamma_{3c}^{ZF}$	2.37	0.0	0.002	M_1
$\Gamma_{1v}^T \rightarrow \Gamma_{4c}^{ZF}$	2.08	0.0	0.0	M_0
$\Gamma_{2v}^T \rightarrow \Gamma_{4c}^{ZF}$	2.09	0.0	0.0	M_0
$\Gamma_{v}^T \rightarrow \Gamma_{4c}^{ZF}$	2.4	0.0	0.0	M_0
$\Gamma_{1v}^T \rightarrow \Gamma_{15c}$	2.43	0.0	0.220	M_0
$\Gamma_{2v}^T \rightarrow \Gamma_{15c}$	2.44	0.0	0.0	M_0
$\Gamma_{v}^z \rightarrow \Gamma_{15c}$	2.75	0.104	0.0	M_0

pared to others, eg., Hybertsen *et al.*[2] and Froyen *et al.*,[3] who get 0.1 and 0.2 eV. However, because even the correct values of these splittings are small, and also, because in each pair of zone-folded states at least one of the states has zero-momentum matrix element with the top valence states (see Table II and also Table II of Ref. 2 and Table III of Ref. 3), we do not expect the above inaccuracy to affect the optical properties noticeably.

III. LINEAR RESPONSE FUNCTION

Within the independent-particle model, the expressions for $\vec{\vec{\epsilon}}_1(\omega)$ and $\vec{\vec{\epsilon}}_2(\omega)$ are given by standard perturbation theory:[21]

$$\vec{\vec{\epsilon}}_2(\omega)=\frac{1}{\pi}\left[\frac{e}{m\omega}\right]^2\sum_{i,j}\int_{BZ} f_{ij}[\mathbf{P}_{ji}\mathbf{P}_{ij}\delta(E_{ji}-\hbar\omega)]d\mathbf{k} , \tag{3.1}$$

$$\vec{\vec{\epsilon}}_1(\omega)=\frac{1}{\pi^2}\left[\frac{\hbar e}{m}\right]^2\sum_{i,j}\int_{BZ}\frac{f_{ij}}{E_{ji}^2}\left[\frac{\mathbf{P}_{ij}\mathbf{P}_{ji}}{(E_{ji}-\hbar\omega)}\right]d\mathbf{k} , \tag{3.2}$$

where $\mathbf{P}_{ij}(\mathbf{k})$ is given by (2.5) and $f_{ij}=f_i-f_j$ are Fermi factor differences. In $\vec{\vec{\epsilon}}_1(\omega)$ there is no singular piece proportional to ω^{-1} because of time-reversal symmetry; the ω^{-2} divergent term vanishes for filled bands because the effective mass tensor is periodic in the Brillouin zone and the integral over the Brillouin zone of the derivative of a periodic function is zero.[22]

We utilize the symmetry groups of even-period (D_{2h}) and odd-period (D_{2d}) strained $(Si)_n/(Ge)_n$ superlattices on Si(001) to take the dielectric tensor to its irreducible form. This is accomplished by applying the operators for the group elements R of the D_{2h} or D_{2d} point groups, P_R, to the expansion dyadics $\hat{i}\hat{j}$ of the dielectric tensor $\vec{\vec{\epsilon}}(\omega)=\sum_{i,j}\epsilon_{ij}\hat{i}\hat{j}$. We find

$$\begin{aligned}
&\sum_R P_R(\hat{x}\hat{x})=\sum_R P_R(\hat{y}\hat{y})=\tau(\hat{x}\hat{x}+\hat{y}\hat{y}) ,\\
&\sum_R P_R(\hat{z}\hat{z})=\mu\hat{z}\hat{z} ,\\
&\sum_R P_R(\hat{i}\hat{j})=0, \quad i\neq j ,
\end{aligned} \tag{3.3}$$

where $i,j=x,y,z$ and $\tau=4,\mu=8$ for even- and $\tau=8,\mu=16$ For odd-period superlattices. The nonvanishing components of $\vec{\vec{\epsilon}}_2(\omega)$ are then given by

$$\epsilon_2^T(\omega)=\frac{\tau}{\pi}\left[\frac{e}{m\omega}\right]^2\sum_{i,j}\int_{IZ} f_{ij}[(P_{ji}^x P_{ij}^x+P_{ji}^y P_{ij}^u)\times\delta(E_{ji}-\hbar\omega)]d\mathbf{k} , \tag{3.4}$$

and

$$\epsilon_2^{zz}(\omega)=\frac{\mu}{\pi}\left[\frac{e}{m\omega}\right]^2\sum_{i,j}\int_{IZ} f_{ij}[P_{ji}^z P_{ij}^z\delta(E_{ji}-\hbar\omega)]d\mathbf{k} , \tag{3.5}$$

where $\epsilon_2^T(\omega)=\epsilon_2^{xx}(\omega)=\epsilon_2^{yy}(\omega)$ and IZ stands for an irreducible segment of the first Brillouin zone (see, e.g., Fig. 1).

We evaluate Eqs. (3.4) and (3.5) using the LATM by dividing the irreducible zone evenly into rectangular parallelopipeds and further reducing these into six constituent tetrahedra. The momentum matrix elements are taken to be constant over each parallelopiped and set equal to the value at the center, while the energies are calculated at the vertices of each tetrahedron.[18] Note that since the Brillouin zone for these superlattices is tetragonal, the irreducible zone is evenly divisible by rectangular parallelepipeds, and there are no difficulties in dealing with the zone boundaries. The integral over constant energy sur-

faces is evaluated with a typical resolution of about 0.02 eV or less, and we typically divide the irreducible zone into 1000 rectangular parallelepipeds.

We obtain $\vec{\vec{\epsilon}}_1(\omega)$ from $\vec{\vec{\epsilon}}_2(\omega)$ by the Kramers-Kronig relation. Our results for $\vec{\vec{\epsilon}}_2(\omega)$ and $\vec{\vec{\epsilon}}_1(\omega)$ are preseted in Figs. 3 and 4, respectively. These are the first evaluations of $\vec{\vec{\epsilon}}(\omega)$ for these superlattices. However, we would like to point out that using a minimal number of orbitals in the linear combination of Gaussian orbitals method, as we have done here, leads to higher conduction bands that are not very accurate even for bulk materials.[1] Also the scheme leads to oscillator strengths that are too small. We expect these deficiencies to carry over into our superlattice calculations. In particular,[22] we expect the real size of the response functions to be considerably scaled up from the values obtained here.

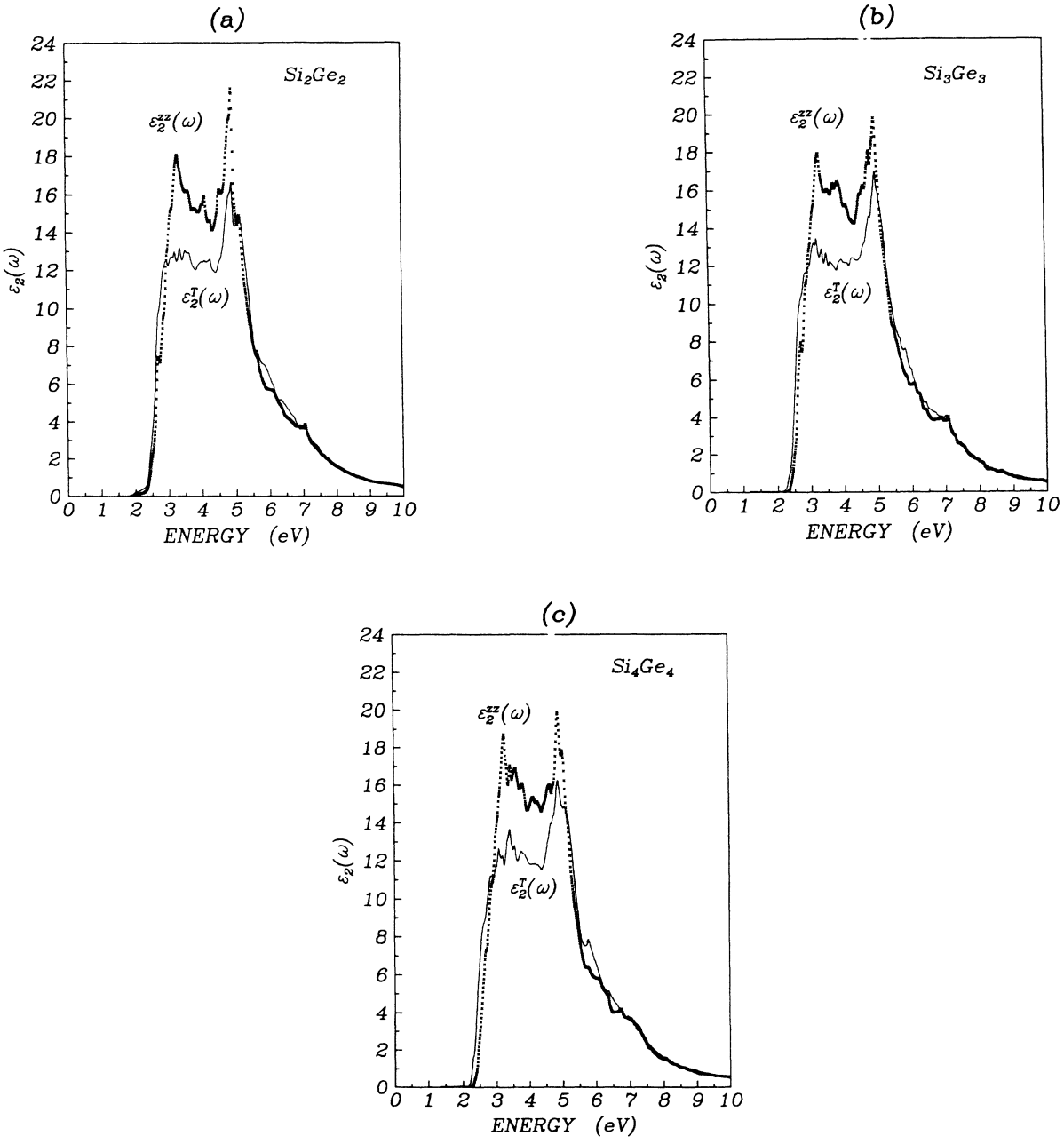

FIG. 3. $\vec{\vec{\epsilon}}_2(\omega)$ for strained $(Si)_n/(GE)_n$ superlattices [solid lines: $\epsilon_2^T(\omega)$; crosses: $\epsilon_2^{zz}(\omega)$]. (a) $(Si)_2/(Ge)_2$, (b) $(Si)_3/(Ge)_3$, (c) $(Si)_4/(Ge)_4$.

IV. RESULTS AND DISCUSSION

A. High-frequency features of $\vec{\epsilon}_1(\omega)$ and $\vec{\epsilon}_2(\omega)$

From Figs. 3 and 4 it is evident that in all the superlattices the main features in $\vec{\epsilon}_1(\omega)$ and $\vec{\epsilon}_2(\omega)$ are very similar at frequencies higher than those near the absorption edges. This is not unexpected: Since the matrix elements between the valence and the folded conduction states are generally 5–20 times smaller than those between the valence and bulk-like conduction states[2] (also see Tables II–IV), one would suspect that the optical response would be dominated by the bulk optical properties of silicon and germanium. This can be verified quantitatively from a simple macroscopic model for the dielectric function of a superlattice, where the superlattice is considered to be constructed from slabs of bulk Si and strained bulk Ge (see Fig. 5). These slabs are assumed to be of finite

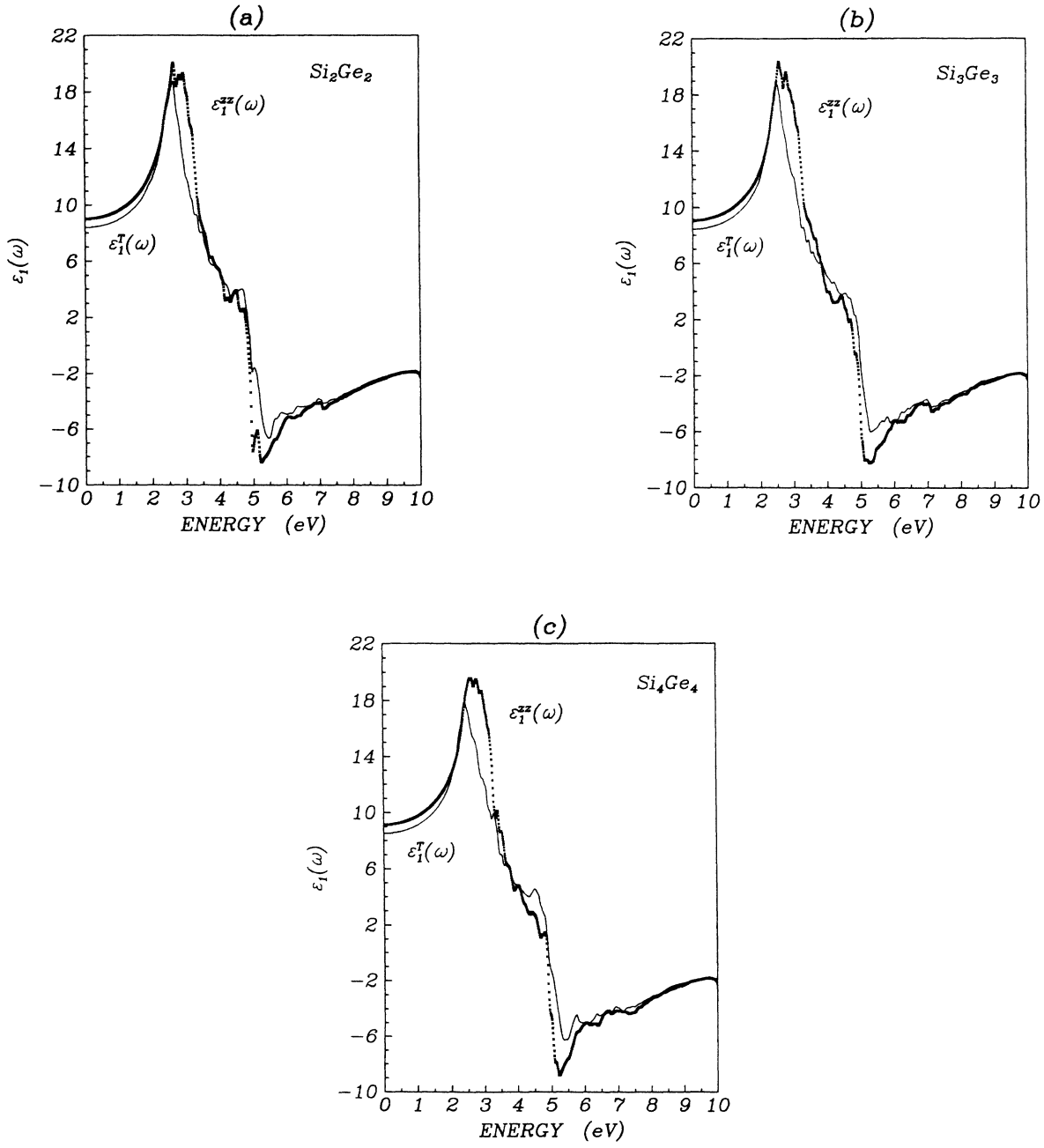

FIG. 4. $\vec{\epsilon}_1(\omega)$ for strained $(Si)_n/(Ge)_n$ superlattices [solid lines: $\epsilon_1^T(\omega)$; crosses: $\epsilon_1^{zz}(\omega)$]. (a) $(Si)_2/(Ge)_2$, (b) $(Si)_3/(Ge)_3$, (c) $(Si)_4/(Ge)_4$.

TABLE III. Critical points at Γ for $(Si)_2/(Ge)_2$ (the labels have been described in the text). $|\langle v|P^T|c\rangle|^2 \equiv \frac{1}{2}(|\langle v|P_x|c\rangle|^2+|\langle v|P_y|c\rangle|^2)$.

Transition	ΔE (eV)	$\lvert\langle v\rvert P^T\rvert c\rangle\rvert^2$ (a.u.)	$\lvert\langle v\rvert P_z\rvert c\rangle\rvert^2$ (a.u.)	Critical point
$\Gamma_{1v}^T \rightarrow \Gamma_{1c}^{ZF}$	1.87	0.056	0.0	M_0
$\Gamma_{2v}^T \rightarrow \Gamma_{1c}^{ZF}$	1.89	0.12	0.0	M_0
$\Gamma_v^z \rightarrow \Gamma_{1c}^{ZF}$	2.19	0.0	0.166	M_0
$\Gamma_{1v}^T \rightarrow \Gamma_{2c}^{ZF}$	2.11	0.0	0.0	M_0
$\Gamma_{2v}^T \rightarrow \Gamma_{2c}^{ZF}$	2.13	0.0	0.0	M_1
$\Gamma_v^z \rightarrow \Gamma_{2c}^{ZF}$	2.43	0.0	0.0	M_0
$\Gamma_{1v}^T \rightarrow \Gamma_{15c}$	2.32	0.173	0.0	M_0
$\Gamma_{2v}^T \rightarrow \Gamma_{15c}$	2.34	0.04	0.0	M_0
$\Gamma_v^z \rightarrow \Gamma_{15c}$	2.63	0.0	0.2	M_0

size but much smaller than the wavelength of the perturbing light beam so that the beam sees an effective dielectric function.

For a transverse applied field $\mathbf{E}_T$ (i.e., normal to the crystal axis which in this case is taken to be the z axis) we have

$$\mathbf{E}_T+\mathbf{E}_T^{Si}=\mathbf{E}_T^{Ge} , \tag{4.1}$$

from the continuity of the tangential electric field across an interface. Therefore, the average induced polarization is given by

$$\mathbf{P}=\tfrac{1}{2}(\mathbf{P}^{Si}+\mathbf{P}^{Ge}) = \frac{1}{2}\left[\frac{\epsilon_{Si}^T-1}{4\pi}+\frac{\epsilon_{Ge}^T-1}{4\pi}\right]\mathbf{E}_T \equiv \left[\frac{\epsilon^T-1}{4\pi}\right]\mathbf{E}_T . \tag{4.2}$$

Using (4.2), the effective dielectric tensor components $\epsilon^{xx}(\omega)=e^{yy}(\omega)$ are given by

$$\epsilon^T(\omega)=\epsilon^{xx}(\omega)=\epsilon^{yy}(\omega)=\tfrac{1}{2}(\epsilon_{Si}^T+\epsilon_{Ge}^T) . \tag{4.3}$$

On the other hand, for a longitudinal field $\mathbf{E}_L=E\hat{\mathbf{z}}$ we have

$$\epsilon^{zz}\mathbf{E}_L=\epsilon_{Si}^{zz}\mathbf{E}_L^{Si}=\epsilon_{Ge}^{zz}\mathbf{E}_L^{Ge} , \tag{4.4}$$

where ϵ^{zz} is the indicated component of the effective dielectric tensor. The averaged induced polarization then is given by

$$\mathbf{P}=\frac{1}{2}\left[\frac{\epsilon_{Si}^{zz}-1}{4\pi\epsilon_{Si}^{zz}}+\frac{e_{Ge}^{zz}-1}{4\pi\epsilon_{Ge}^{zz}}\right]\frac{\mathbf{E}_L}{\epsilon^{zz}} . \tag{4.5}$$

Therefore, we have

$$\frac{\epsilon^{zz}-1}{\epsilon^{zz}}=\frac{1}{2}\left[\frac{\epsilon_{Si}^{zz}-1}{\epsilon_{Si}^{zz}}+\frac{\epsilon_{Ge}^{zz}-1}{\epsilon_{Ge}^{zz}}\right] , \tag{4.6}$$

yielding

$$\epsilon^{zz}=\frac{2\epsilon_{Si}^{zz}\epsilon_{Ge}^{zz}}{\epsilon_{Si}^{zz}+\epsilon_{Ge}^{zz}} . \tag{4.7}$$

To evaluate the macroscopic response functions (4.3) and (4.7) one needs $\vec{\epsilon}_1(\omega)$ and $\vec{\epsilon}_2(\omega)$ for bulk Si and strained Ge. We calculate the band structures of bulk Si and uniaxially stressed Ge (with lattice constants as given in Table V) in the same manner as in the superlattice using the minimal basis LCGO approach. The band structure of silicon obtained from the minimal basis LCGO method has already been presented and discussed by Huang *et al.*,[12] and will not be repeated here. We present the band structure of strained Ge in Fig. 6(a) and the corresponding $\vec{\epsilon}_2(\omega)$ and $\vec{\epsilon}_1(\omega)$ in Fig. 7.

Using these results and Eqs. (4.3) and (4.7), we obtain macroscopic estimates for the effective $\vec{\epsilon}_1(\omega)$ and $\vec{\epsilon}_2(\omega)$. The results are presented in Fig. 8. Comparing these results and the microscopic calculation (Figs. 3 and 4), it is evident that the main features (including the anisotropy) are well reproduced by this simple macroscopic model. This indicates that the prominent features of $\epsilon_2^T(\omega)$ and $\epsilon_2^{zz}(\omega)$ in all of the superlattices studied here indeed arise mostly from bulklike transitions. In particular, the two main peaks correspond to E_1 and E_2 peaks in bulk Si and Ge. Note that in the superlattices these peaks are broader and weaker than the corresponding peaks in the

TABLE IV. Critical points at Γ for Si_3/Ge_3 (the labels have been described in the text). $|\langle v|P^T|c\rangle|^2 \equiv \frac{1}{2}(|\langle v|P_x|c\rangle|^2+|\langle v|P_y|c\rangle|^2)$.

Transition	ΔE (eV)	$\lvert\langle v\rvert P^T\rvert c\rangle\rvert^2$ (a.u.)	$\lvert\langle v\rvert P_z\rvert c\rangle\rvert^2$ (a.u.)	Critical point
$\Gamma_v^T \rightarrow \Gamma_{1c}^{ZF}$	1.22	0.0	0.0	M_1
$\Gamma_v^z \rightarrow \Gamma_{1c}^{ZF}$	1.54	0.0	0.0	M_1
$\Gamma_v^T \rightarrow \Gamma_{2c}^{ZF}$	1.22	0.0	0.0	M_0
$\Gamma_v^z \rightarrow \Gamma_{2c}^{ZF}$	1.54	0.0	0.0	M_0
$\Gamma_v^T \rightarrow \Gamma_{15c}$	2.10	0.170	0.0	M_0
$\Gamma_v^z \rightarrow \Gamma_{15c}$	2.42	0.0	0.367	M_0

TABLE V. Lattice constants in Å.

Substrate	a_z	a_T^{Si}	a_T^{Ge}
Si	5.43	5.43	5.82

constituent bulk materials. This is particularly true for $\epsilon_2^T(\omega)$ where, in the macroscopic model, the response is a simple average of the bulk response. Since the $\vec{\epsilon}_2(\omega)$ peaks in bulk Si and Ge are at slightly different frequencies, the averaging broadens and weakens the $\epsilon_2^T(\omega)$ peaks in superlattices; since the E_1 peak in Si occurs about 1 eV higher than in Ge, the corresponding E_1 peak in superlattices is very broad and weak, while the E_2 peak, which occurs more or less at same frequency in both bulk materials, is a sharp and large peak in the superlattices. The features of $\epsilon_2^{zz}(\omega)$ arise from a more complicated function of bulk properties, and the frequency shifts of the peaks are not very important.

B. Source and size of the anisotropy

From the above result it is also evident that the most of the anisotroppy is due the bulk properties. To illustrate this point further we repeat the macroscopic calculation with no strain in Ge (see Fig. 9). In this case the calculated anisotropy almost completely vanishes. Therefore, away from the absorption edges, the anisotropy in the superlattices is mostly due to the strain in the Ge.

The relative magnitudes of $\epsilon_2^T(\omega)$ and $\epsilon_2^{zz}(\omega)$ in the superlattices can thus be understood if one can explain the relative magnitudes of the corresponding response functions in strained Ge. The effects of strin on the band structure and momentum matrix elements, and therefore the optical properties, is complicated.[23] To seek a simple physical explanation for the anisotropy that we have calcualted here, we consider an empirical bonding-antibonding tight-binding model,[24,25] which is simple and physically very intuitive. Assuming that the momentum matrix element at any point in the Brillouin zone can be replaced by an average momentum matrix element,[26] the expression for $\vec{\epsilon}_2(\omega)$ in this model becomes

$$\epsilon_2^{\alpha\alpha}(\omega)=\frac{1}{\pi}\left[\frac{e}{m\omega}\right]^2|\langle P^\alpha\rangle|^2\sum_{i,j}\int_{BZ}f_{ij}\delta(E_{ji}-\hbar\omega)d\mathbf{k}\ , \tag{4.8}$$

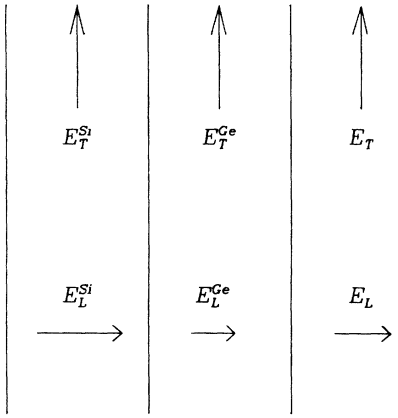

FIG. 5. A macroscopic model for the superlattices.

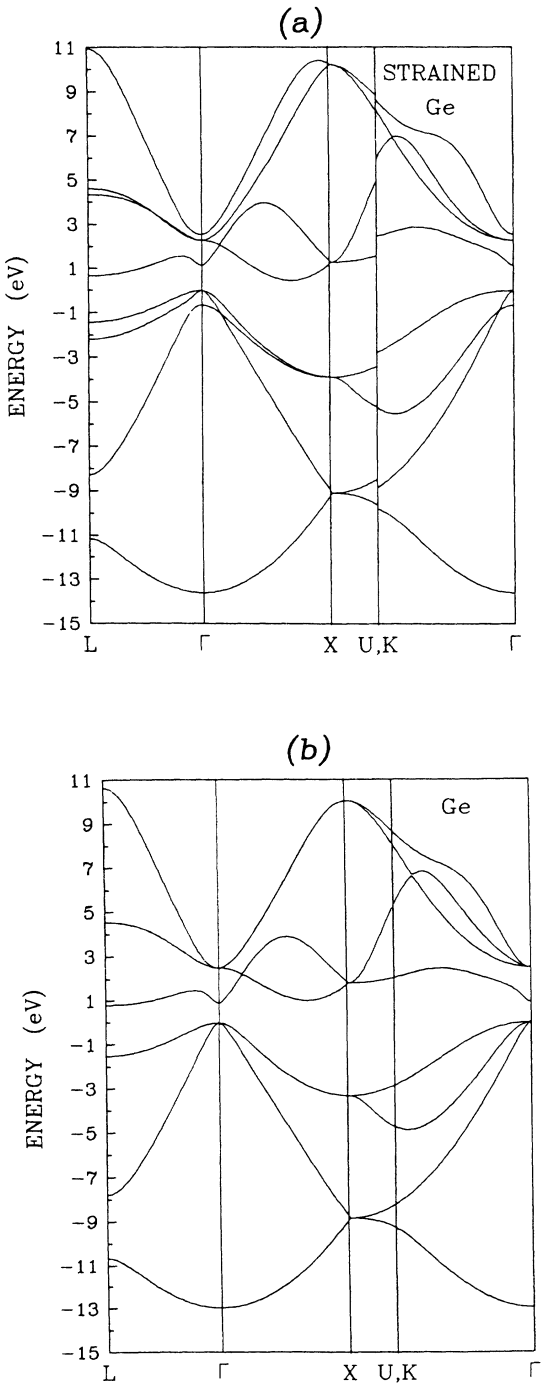

FIG. 6. Energy band structure of bulk materials. (a) Bulk strained Ge (note that because of strain the U and K points are not equivalent), (b) bulk Ge.

where

$$|\langle P^{\alpha}\rangle|^2 \propto (t_{\alpha})^2 = \left[\frac{a_{\alpha}}{4}\right]^2, \quad \alpha = x,y,z \ , \tag{4.9}$$

and where t^{α} is the αth component of the bond (antibond) vector which points along a bond (antibond) between two atomic sites in a unit cell; a_{α} is the lattice constant in the αth direction. Now, in a cubic bulk material such as Ge, we have $t_x^2 = t_y^2 = t_z^2$ and therefore the material is optically isotropic. When Ge is uniaxially stressed we have

$$\epsilon_2^T(\omega) = \epsilon_2^{xx}(\omega) = \epsilon_2^{yy}(\omega) \propto \left[\frac{a_T}{4}\right]^2 ,$$
$$\epsilon_2^{zz}(\omega) \propto \left[\frac{a_z}{4}\right]^2 . \tag{4.10}$$

Using the values of Table V we find

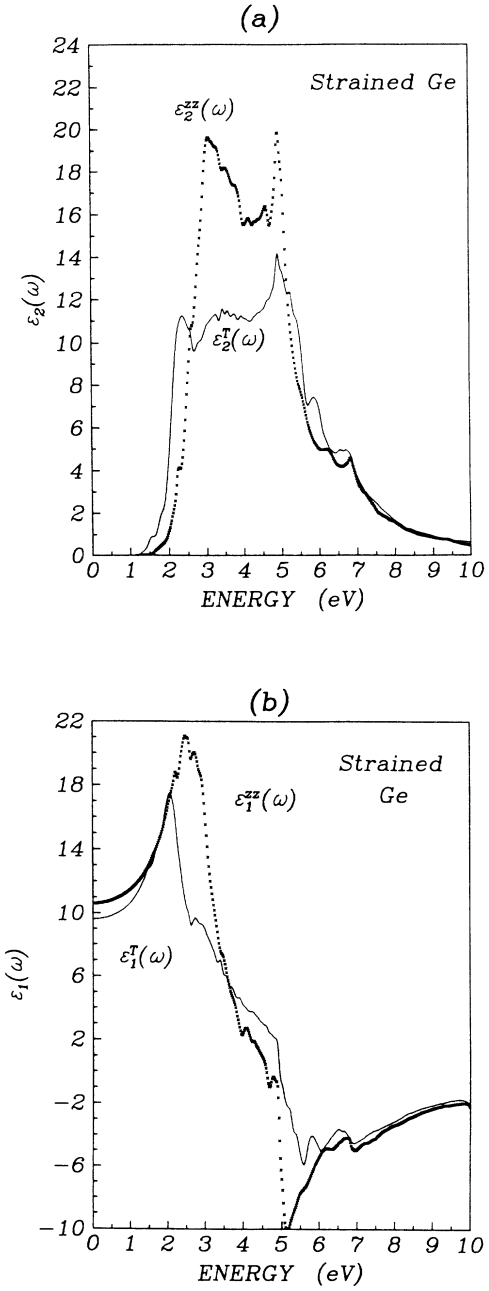

FIG. 7. Dielectric function for strained Ge [solid lines: $\epsilon_2^T(\omega)$, $\epsilon_1^T(\omega)$; crosses: $\epsilon_2^{zz}(\omega)$, $\epsilon_1^{zz}(\omega)$]. (a) $\vec{\epsilon}_2(\omega)$, (b) $\vec{\epsilon}_1(\omega)$.

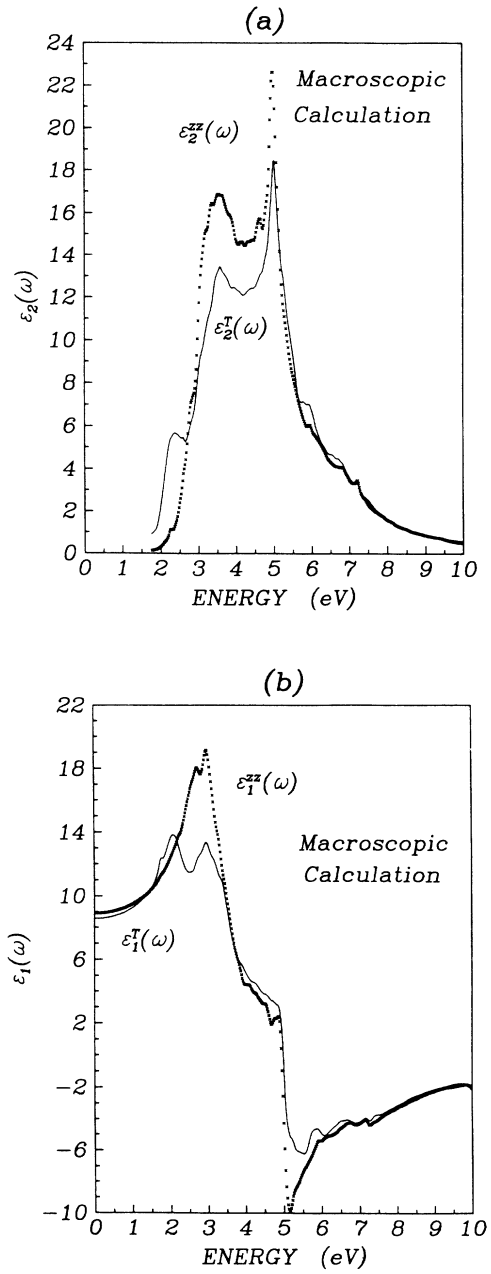

FIG. 8. Macroscopic calculation with Ge strained [solid lines: $\epsilon_2^T(\omega)$, $\epsilon_1^T(\omega)$; crosses: $\epsilon_2^{zz}(\omega)$, $\epsilon_1^{zz}(\omega)$]. (a) $\vec{\epsilon}_2(\omega)$, (b) $\vec{\epsilon}_1(\omega)$.

$$\frac{\epsilon_2^{zz}(\omega)}{\epsilon_2^{T}(\omega)} \approx 1.15 \ . \tag{4.11}$$

Although in reality the anisotropy is a complicated function of frequency, and varies from 0 to about 50% (see Fig. 7), we see from this simple argument that solely from the bond (antibond) orientation in the strained material we can expect a 15% anisotropy.

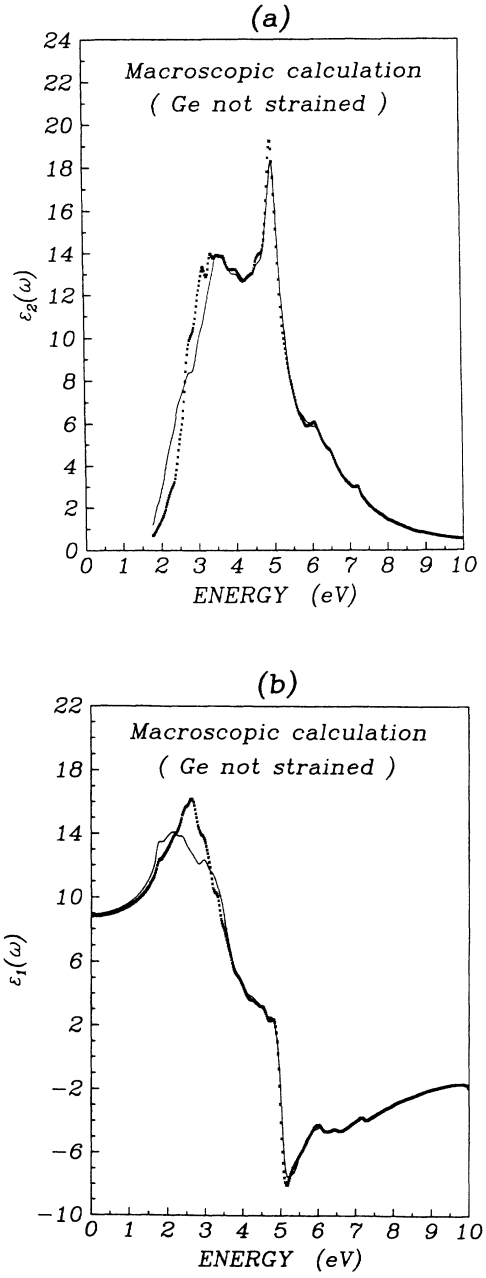

FIG. 9. Macroscopic calculation with Ge no strained [solid lines: $\epsilon_2^T(\omega)$, $\epsilon_1^T(\omega)$; crosses: $\epsilon_2^{zz}(\omega)$, $\epsilon_1^{zz}(\omega)$]. (a) $\vec{\epsilon}_2(\omega)$, (b) $\vec{\epsilon}_1(\omega)$.

C. Unique superlattice features

The superlattice optical properties differ from the bulklike properties at the absorption edge due to new transitions to the folded bands. However, the magnitude of the $\vec{\epsilon}_2(\omega)$ at these frequencies is about 2 orders of magnitude smaller than bulklike features at higher frequencies, due to the fact that the momentum matrix element between zone-folded (ZF) states is about an order of magnitude smaller than the bulklike matrix elements. Because we employ the LATM, in which the momentum matrix elements are approximated as uniform over each rectangular parallelepiped and equal to their value at the center of the parallelepiped, the actual shape of the response function is not accurately given at the absorption edge. To examine the nature of the band edges more carefully, we have evaluated the effective masses at the band edges and determined the nature of the critical points. The results are summarized in Tables II–IV, where we use the following labeling scheme: The Γ_{15c} is a bulklike conduction state corresponding to usual Γ_{15} state in the bulk zinc-blende semiconductors. The Γ_{1c}^{ZF}, Γ_{2c}^{ZF}, Γ_{3c}^{AF}, and Γ_{4c}^{ZF} are the first, second, third, and fourth zone-folded states in increasing order of energy. The triply degenerate bulk valence $\Gamma_{25'v}$ state is split by the tetragonal deformation into a p_z-like state, labeled by Γ_v^z, and two p_x,p_y like states. The later states are degenerate for $n=3$ (labeled Γ_v^T), but are split for $n=2,4$ because of the missing fourfold rotation axis. In the latter case these states are labeled by Γ_{2v}^T and Γ_{1v}^T in increasing order of energy. From these results it is evident that the real signature of each superlattice occurs only at the superlattice absorption edges. However, this signature is very weak and it would be hard to detect in a simple absorption experiment due to contributions from the indirect transitions in the bulk substrate.

In conclusion then, we have carried out the first full band-structure calculation of the linear optical properties of the strained $(Si)_n/(Ge)_n$ (001) superlattices. We have used a simple macroscopic calculation to show that most of the features of the response function at frequencies away from the absorption edge are due to bulk-like transitions. We found that the expected anisotropy in these novel materials is large and almost entirely due to the strain in Ge. In a simple model the larger size of response in the direction of the superlattice axis is due to the fact that the bonds (antibonds) are mainly aligned in this direction. The pure superlattice features are only observed near the absorption edges. These features differ from superlattice to superlattice, and are the real signature of each superlattice.

ACKNOWLEDGMENTS

We wish to thank Professor W. Y. Ching for providing us with his data for the tight-binding orbitals and potentials of bulk Si and Ge. We would like also to thank Dr. C. M. de Sterke for his helpful comments. We gratefully acknowledge research support from the Natural Sciences and Engineering Research Council (NSERC) of Canada. This work was partially supported by Ontario Laser and Lightwave Research Centre.

APPENDIX A: ANALYTIC EXPRESSIONS FOR THE MULTICENTER GAUSSIAN INTEGRALS

As pointed out in the text, all integrals involved in the construction of the overlap and Hamiltonian and momentum matrix elements can be evaluated analytically. The full derivations of analytic results of this type are discussed by Sanders.[16] Below we only present the final expressions.

Let $\mathbf{r}_A$ denote a distance between a point A with coordinates (A_x, A_y, A_z) and a field point (x,y,z). Vector $\mathbf{r}_A$ is then given by

$$\mathbf{r}_A=(x-A_x)\hat{\mathbf{x}}+(y+A_y)\hat{\mathbf{y}}+(z-A_z)\hat{\mathbf{z}} =x_A\hat{\mathbf{x}}+y_A\hat{\mathbf{y}}+z_A\hat{\mathbf{z}} . \tag{A1}$$

Then a general Gaussian-type orbital centered on A is defined as follows

$$G(\alpha_m, \mathbf{A},p_1,q_1,s_1)=x_A^{p_1}y_A^{q_1}z_A^{s_1}e^{-\alpha_m \mathbf{r}_A^2} . \tag{A2}$$

The overlap integral between two Gaussians centered on points A and B (a two-center integral) is given by

$$\int d\mathbf{r}\, G(\alpha_m, \mathbf{A},p_1,q_1,s_1)G(\alpha_n,\mathbf{B},p_2,q_2,s_2)=\zeta I_x I_y I_z , \tag{A3}$$

where

$$\zeta=e^{-(\alpha_m AP^2+\alpha_n BP^2)} ,$$

$$\mathbf{P}=\frac{\alpha_m \mathbf{A}+\alpha_n \mathbf{B}}{\alpha_T} ,$$

$$A\mathbf{P}=\mathbf{P}-\mathbf{A} ,$$

$$\alpha_T=\alpha_m+\alpha_n$$

$$I_x(\alpha_T, AP_x,BP_x)=\left[\frac{\pi}{\alpha_T}\right]^{1/2}\sum_{i=0}^{\lfloor (p_1+p_2)/2\rfloor} f_{2i}(p_1,p_2, AP_x,BP_x)\frac{(2i-1)!!}{(2\alpha_T)^i} ,$$

$$f_k(p_1,p_2, AP_x,BP_x)=\sum_{j=0}^{p_1}\sum_{l=0}^{p_2}\delta_{j+l,k}(AP_x)^{p_1-1}\begin{bmatrix}p_1\\ j\end{bmatrix}(BP_x)^{p_2-1}\begin{bmatrix}p_2\\ l\end{bmatrix} ,$$

$$\begin{bmatrix}p_1\\ j\end{bmatrix}=\frac{p_1!}{j!(p_1-j)!} ,$$

and similar expressions for I_y and I_z. Note that, the notation $[p/2]$ indicates the largest integer part of $p/2$ and $\delta_{j+l,k}$ is Kronecker δ.

The overlap between two Gaussian-type orbitals centered at A and B with a Gaussian $e^{\gamma_w \mathbf{r}_c^2}$ (a three-center integral), of the type appearing in the last term of Eq. (2.4), is similarly given by

$$\int d\mathbf{r}\, G(\alpha_m, \mathbf{A},p_1,q_1,s_1)e^{\gamma_w \mathbf{r}_c^2}G(\alpha_n,\mathbf{B},p_2,q_2,s_2)=\eta I_x(\alpha_T, AE_x,BE_x)I_y(\alpha_T, AE_z,BE_y)I_z(\alpha_T, AE_z,BE_z) , \tag{A4}$$

where

$$\eta=e^{-(\alpha_m AE^2+\alpha_n BE^2+\gamma_w CE^2)} ,$$

$$\mathbf{E}=\frac{\alpha_m \mathbf{A}+\alpha_n \mathbf{B}+\gamma_w \mathbf{C}}{\alpha_T} ,$$

$$\alpha_T=\alpha_m+\alpha_n+\gamma_w .$$

The kinetic and momentum integrals are expressed in terms of two-center overlap integrals as follows. For the kinetic integral we have

$$\int d\mathbf{r}\, G(\alpha_m, \mathbf{A},p_1,q_1,s_1)(-\tfrac{1}{2}\nabla^2)G(\alpha_n,\mathbf{B},p_2,q_2,s_2)=J_x+J_y+J_z , \tag{A5}$$

where

$$J_x=\alpha_n(2p_2+1)\int d\mathbf{r}\, G(\alpha_m, \mathbf{A},p_1,q_1,s_1)G(\alpha_n,\mathbf{B},p_2,q_2,s_2)-2\alpha_n^2\int d\mathbf{r}\, G(\alpha_m, \mathbf{A},p_1,q_1,s_1)G(\alpha_n,\mathbf{B}, p_2+2, q_2,s_2)$$

$$-\frac{p_2(p_2-1)}{2}\int d\mathbf{r}\, G(\alpha_m, \mathbf{A},p_1,,q_1,s_1)G(\alpha_n,\mathbf{B}, p_2-2,q_2,s_2)$$

and similar expressions for J_y and J_z. The momentum integrals are given by

$$\int d\mathbf{r}\, G(\alpha_m, \mathbf{A}, p_1, q_1, s_1)\frac{\partial}{\partial x}G(\alpha_n, \mathbf{B}, p_2, q_2, s_2) = p_2 \int d\mathbf{r}\, G(\alpha_m, \mathbf{A}, p_1, q_1, s_1)G(\alpha_n, \mathbf{B}, p_2-1, q_2, s_2) - 2\alpha_n \int d\mathbf{r}\, G(\alpha_m, \mathbf{A}, p_1, q_1, s_1)G(\alpha_n, \mathbf{B}, p_2+1, q_2, s_2) \tag{A6}$$

with similar expressions for the $\partial/\partial y$ and $\partial/\partial z$ terms.

The Coulomb integral is given by

$$\begin{aligned}\int d\mathbf{r}\, G(\alpha_m, \mathbf{A}, p_1, q_1, s_1)\frac{e^{-\beta r_c^2}}{|\mathbf{r}_c|}G(\alpha_n, \mathbf{B}, p_2, q_2, s_2) &= \frac{2\pi}{\alpha_T}\Xi \sum_{p=0}^{p_1+p_2}(-1)^p \varepsilon^{p/2} p! f_p(p_1, p_2, AE_x, BE_x) \sum_{a=0}^{\lfloor p/2 \rfloor}\frac{1}{a!}\sum_{t=0}^{\lfloor L/2 \rfloor}\frac{(-1)^t (CE_x)^{L-2t}}{t!(L-2t)!}\varepsilon^{t-L/2} \\ &\times \sum_{q=0}^{q_1+q_2}(-1)^q \varepsilon^{q/2} q! f_q(q_1, q_2, AE_y, BE_y) \sum_{b=0}^{\lfloor q/2 \rfloor}\frac{1}{b!}\sum_{u=0}^{\lfloor M/2 \rfloor}\frac{(-1)^u (CE_y)^{M-2u}}{u!(M-2u)!}\varepsilon^{u-M/2} \\ &\times \sum_{s=0}^{s_1+s_2}(-1)^s \varepsilon^{s/2} s! f_s(s_1, s_2, AE_z, BE_z) \sum_{c=0}^{\lfloor s/2 \rfloor}\frac{1}{c!}\sum_{v=0}^{\lfloor N/2 \rfloor}\frac{(-1)^s (CE_z)^{N-2v}}{v!(N-2v)!}\varepsilon^{v-N/2} \\ &\times F_{L-t+M-u+N-v}(\alpha_T C E^2)\,,\end{aligned} \tag{A7}$$

where

$$\varepsilon = \frac{1}{4\alpha_T}\,,$$

$$L \equiv p - 2a\,,$$

$$M \equiv q - 2b\,,$$

$$N \equiv s - 2c\,,$$

$$\alpha_T = \alpha_m + \alpha_n + \beta\,,$$

$$\mathbf{E} = \frac{\alpha_m \mathbf{A} + \alpha_n \mathbf{B} + \beta \mathbf{C}}{\alpha_T}\,,$$

$$\Xi = e^{-(\alpha_m AE^2 + \alpha_n BE^2 + \beta CE^2)}\,,$$

$$F_h(Q) = \int_0^1 dw\, e^{-Qw^2} w^{2h}\,.$$

Note that the function $F_h(Q)$ satisfies the recursion relation

$$F_{h+1}(Q) = [(2h+1)F_h(Q) - e^{-Q}]\frac{1}{2Q} \tag{A8}$$

and is related to the error function

$$F_0(\phi^2) = \frac{\sqrt{\pi}}{2}\frac{\mathrm{erf}(\phi)}{\phi}\,. \tag{A9}$$

APPENDIX B: THE ORTHOGONALIZATION TO CORE BLOCH STATES

Let $|b_\Delta\rangle_V$ be the abstract state representing the three-dimensional superlattice valence Bloch (VB) state of the atoms of type (Δ). Similarly, $|b_\Lambda\rangle_C$ represents a core Bloch state (CB) of the atoms of type (Λ). We construct a new VB state $|b_\Delta^0\rangle_B$ as follows:

$$|b_\Delta^0\rangle_B = |b_\Delta\rangle_B + \sum_\Theta \sum_{C'(\Theta)} \mathcal{A}_{\Delta,V;\Theta,C'} |b_\Theta\rangle_{C'}\,. \tag{B1}$$

The condition for orthogonality requires that

$$\langle b_\Delta^0 | b_\Omega \rangle_{VC} = 0\,. \tag{B2}$$

Substituting (B1) into (B2) we get

$$\langle b_\Delta | b_\Omega \rangle_{VC} + \sum_\Theta \sum_{C'\Theta} \mathcal{A}_{\Delta,V;\Theta,C'} \langle b_\Theta | b_\Omega \rangle_{C'C} = 0\,. \tag{B3}$$

To determine the coefficients $\mathcal{A}$ a series of simultaneous equations must be solved. However, since the overlap between different core states is small we assume

$$\langle b_\Theta | b_\Omega \rangle_{C'C} = \delta_{C',C}\delta_{\Theta,\Omega}\,. \tag{B4}$$

With the above approximation (B3) gives

$$\mathcal{A}^*_{\Delta,V;\Omega,C} = -\langle b_\Delta | b_\Omega \rangle_{VC}\,. \tag{B5}$$

Substituting (B5) into (B1) we get

$$|b_\Delta^0\rangle_B = |b_\Delta\rangle_V - \sum_\Theta \sum_{C(\Theta)} |b_\Theta\rangle_C \langle b_\Theta | b_\Delta \rangle_{CV}\,. \tag{B6}$$

In the actual calculation the orgonalization procedure is applied to the Hamiltonian, overlap, and momentum matrices. In the new basis the Hamiltonian matrix is given by

$$(H_{\Lambda,\Delta})_{\nu'\nu} \equiv \langle b^0_\Lambda | H | b^0_\Delta \rangle_{\nu'\nu}$$
$$= \langle b_\Lambda | H | b_\Delta \rangle_{\nu'\nu} - \sum_{\Omega} \sum_{C(\Omega)} \langle b_\Lambda | H | b_\Omega \rangle_{\nu' C} \langle b_\Omega | b_\Delta \rangle_{C\nu} - \sum_{\Theta} \sum_{C'(\Theta)} \langle b_\Lambda | b_\Theta \rangle_{\nu' C'} \langle b_\Theta | H | b_\Delta \rangle_{C'\nu}$$
$$+ \sum_{\Omega} \sum_{C(\Omega)} \sum_{\Theta} \sum_{C'(\Theta)} \langle b_\Lambda | b_\Theta \rangle_{\nu' C'} \langle b_\Theta | H | b_\Omega \rangle_{C' C} \langle b_\Omega | b_\Delta \rangle_{C\nu} \, . \tag{B7}$$

The momentum and overlap matrix in the new basis are obtained similarly.

[1] E. Ghaharamani and J. E. Sipe, Phys. Rev. B **40**, 1102 (1989).

[2] M. S. Hybertsen and M. Schlüter, Phys. Rev. B **36**, 9683 (1987); M. S. Hypertsen and S. G. Louie, *ibid.* **34**, 5390 (1986).

[3] S. Froyen, D. M. Wood, and A. Zunger, Phys. Rev. B **36**, 4547 (1987); **37**, 6893 (1988).

[4] I. Morrison and M. Jaros, Phys. Rev. B **37**, 916 (1988); K. B. Wong, M. Jaros, I. Morrison, and J. P. Hagon, Phys. Rev. Lett. **60**, 2221 (1988).

[5] S. Circai and I. P. Batra, Phys. Rev. B **38**, 1835 (1988).

[6] T. P. Pearsall, J. Bevk, L. C. Feldman, J. M. Bonar, J. P. Mannaerts, and A. Ourmazd, Phys. Rev. Lett. **58**, 729 (1987); J. Bevk, A. Ourmazd, L. C. Feldman, T. P. Pearsall, J. M. Bonar, B. A. Davdson, and J. P. Mannaerts, Appl. Phys. Lett. **50**, 760 (1987).

[7] M. S. Hybertsen, M. Schlüter, R. People, S. A. Jachson, D. V. Lang, T. P. Pearsall, J. C. Bean, J. M. Vandenberg, and J. Bevk, Phys. Rev. B **37**, 10 195 (1988).

[8] T. P. Pearsall, J. Bevk, J. M. Bonar, J. P. Mannaerts, and A. Ourmazd, Phys. Rev. B **39**, 3741 (1989).

[9] J. A. Appelbaum and J. R. Hamann, Inst. Phys. Conf. Ser. **39**, 111 (1978); P. J. Feibelmann, J. A. Appelbaum, and D. R. Hamann, Phys. Rev. B **20**, 1433 (1979).

[10] W. Y. Ching and C. C. Lin, Phys. Rev.B **12**, 5536 (1975).

[11] C. S. Wang and J. Callaway, Comput. Phys. Commun. **14**, 327 (1978).

[12] C. S. Wang and B. M. Klien, Phys. Rev. B **24**, 3417 (1981).

[13] B. N. Harmon and W. Weber, Phys. Rev. B **25**, 1109 (1982).

[14] M. Z. Huang and W. Y. Ching, J. Phys. Chem. Solids **46**, 977 (1985), and references therein.

[15] J. von Boehm, P. Kuivalainen, and J. L. Calais, Phys. Rev. B **35**, 8177 (1987).

[16] V. R. Sanders, in *Computational Techniques in Quantum Chemistry and Molecular Physics,* edited by G. H. F. Diercksen, B. T. Sutcliffe, and A. Veillard (Riedel, Dordercht, 1975), p. 347.

[17] V. R. Sanders, in *Methods in Computational Physics,* edited by G. H. F. Diercksen and S. Wilson (Riedel, Dordercht, 1983).

[18] D. J. Moss, J. E. Sipe, and H. M. van Driel, Phys. Rev. B **36**, 1153 (1987), and references therein.

[19] E. Clementi and C. Roetti, At. Data Nucl. Data Tables **14**, 3 (1974).

[20] P. Hohenberg and W. Kohn, Phys. Rev. **136**, B864 (1964); W. Kohn and L. J. Sham, Phys. Rev. **140**, A1133 (1965).

[21] F. Wooten, *Optical Properties of Solids* (Academic, New York, 1972),

[22] See, e.g., D. J. Moss, E. Ghaharamani, J. E. Sipe, and H. M. van Driel, Phys. Rev. B **41**, 1542 (1990).

[23] See, X. Zhau, S. Fahy, and S. G. Louie, Phys. Rev. B **39**, 7840 (1989); I. Gorczyca, N. E. Christensen, and M. Alouani, *ibid.* **39**, 7705 (1989); D. J. Dunstan and B. Gil *ibid.* **38**, 7862 (1988); A. R. Goni, K. Strössner, K. Syassen, and M. Cardona, *ibid.* **36**, 1581 (1987).

[24] W. A. Harrison, *Electronic Structures and the Properties of Solids* (Freeman, San Francisco, 1980).

[25] D. J. Moss, E. Ghaharamani, J. E. Sipe, and H. M. van Driel, Phys. Rev. B **34**, 8758 (1986).

[26] See, for instance, Ref. 21, pp. 114 and 115.